






RESEARCH ARTICLE | SEPTEMBER 12 2023

## Experimental study of turbulent thermal diffusion of particles in an inhomogeneous forced convective turbulence

E. Elmakies ; O. Schildkrot; N. Kleeorin ; A. Levy ; I. Rogachevskii  



*Physics of Fluids* 35, 095123 (2023)

<https://doi.org/10.1063/5.0163878>



CrossMark



### APL Bioengineering

## Special Topic: Drug/Gene Delivery and Theranostics

**Read Now!**

 AIP  
Publishing

# Experimental study of turbulent thermal diffusion of particles in an inhomogeneous forced convective turbulence

Cite as: Phys. Fluids **35**, 095123 (2023); doi: [10.1063/5.0163878](https://doi.org/10.1063/5.0163878)

Submitted: 19 June 2023 · Accepted: 25 August 2023 ·

Published Online: 12 September 2023



View Online



Export Citation



CrossMark

E. Elmakies, O. Shildkrot, N. Kleeorin, A. Levy, and I. Rogachevskii<sup>a)</sup>

## AFFILIATIONS

The Pearlstone Center for Aeronautical Engineering Studies, Department of Mechanical Engineering, Ben-Gurion University of the Negev, P. O. Box 653, Beer-Sheva 8410530, Israel

<sup>a)</sup> Author to whom correspondence should be addressed: [gary@bgu.ac.il](mailto:gary@bgu.ac.il)

## ABSTRACT

We investigate experimentally the phenomenon of turbulent thermal diffusion of micrometer-size solid particles in an inhomogeneous convective turbulence forced by one vertically oriented oscillating grid in an air flow. This effect causes the formation of large-scale inhomogeneities in particle spatial distributions in a temperature-stratified turbulence. We perform detailed comparisons of the experimental results with those obtained in our previous experiments with an inhomogeneous and anisotropic stably stratified turbulence produced by a one oscillating grid in the air flow. Since the buoyancy increases the turbulent kinetic energy for convective turbulence and decreases it for stably stratified turbulence, the measured turbulent velocities for convective turbulence are larger than those for stably stratified turbulence. This tendency is also seen in the measured vertical integral turbulent length scales. Measurements of temperature and particle number density spatial distributions show that particles are accumulated in the vicinity of the minimum of the mean temperature due to the phenomenon of turbulent thermal diffusion. This effect is observed in both convective and stably stratified turbulence, where we find the effective turbulent thermal diffusion coefficient for micrometer-size particles. The obtained experimental results are in agreement with theoretical predictions.

© 2023 Author(s). All article content, except where otherwise noted, is licensed under a Creative Commons Attribution (CC BY) license (<http://creativecommons.org/licenses/by/4.0/>). <https://doi.org/10.1063/5.0163878>

## I. INTRODUCTION

Turbulent transport of particles has been a subject of many studies due to numerous applications in geophysics and environmental sciences, astrophysics, and various industrial flows.<sup>1–7</sup> Different mechanisms of large-scale and small-scale clustering of inertial particles have been proposed. The large-scale clustering occurs in scales that are much larger than the integral scale of turbulence, while the small-scale clustering is observed in scales that are much smaller than the integral turbulence scale.

The large-scale clustering of inertial particles in the isothermal non-stratified inhomogeneous turbulence occurs due to turbophoresis,<sup>8–13</sup> which is a combined effect of particle inertia and inhomogeneity of turbulence. Turbophoresis results in the appearance of the additional non-diffusive turbulent flux of inertial particles  $J_{\text{turboph}} = \bar{n} \bar{V}_{\text{turboph}}$ , where the mean particle velocity caused by turbophoresis can be written as

$$\bar{V}_{\text{turboph}} = -\kappa_{\text{turb}} \frac{\nabla \langle u^2 \rangle}{2}. \quad (1)$$

Here,  $\bar{n}$  is the mean number density of inertial particles,  $\mathbf{u}$  is the turbulent fluid velocity,  $\kappa_{\text{turb}}$  is the turbophoretic coefficient, which generally depends on the Stokes number  $St = \tau_p / \tau_\nu$  and the fluid Reynolds number  $Re = \ell_0 u_{\text{rms}} / \nu$ , where  $\tau_\nu = \tau_0 / Re^{1/2}$  is the Kolmogorov viscous time,  $\tau_0 = \ell_0 / u_{\text{rms}}$  is the characteristic turbulent time,  $\nu$  is the kinematic viscosity,  $u_{\text{rms}} \equiv \sqrt{\langle u^2 \rangle}$  is the rms velocity in the integral turbulence scale  $\ell_0$ , and  $\tau_p$  is the Stokes time for the small spherical particles. Due to turbophoresis, inertial particles are accumulated in the vicinity of the minimum of the turbulent intensity. In particular, direct numerical simulations (DNS)<sup>13</sup> show that inertial particles in inhomogeneously forced isothermal turbulent flows are accumulated at the minima of turbulent velocity. Two turbulent transport processes, turbophoresis and turbulent diffusion, determine the spatial distribution of the particles. Numerical simulations<sup>13</sup> demonstrate that the non-dimensional product of the turbophoretic coefficient  $\kappa_{\text{turb}}$  and the rms velocity  $u_{\text{rms}}$  increases linearly with the parameter  $St_f$  for  $St_f \ll 1$ , reaches a maxima for  $St_f \sim 10$ , and decreases as  $St_f^{-1/3}$  for large  $St_f$ , where  $St_f = \tau_p / \tau_0$  is the Stokes number defined using the

characteristic flow time scale  $\tau_0$  based on the forcing scale of turbulence. The same large-scale clustering phenomenon caused by turbophoresis has been studied in the DNS of turbulent Kolmogorov flows.<sup>14</sup> Although the authors do not interpret their results as a balance between turbophoretic and turbulent diffusive fluxes, they do observe that the large-scale clustering increases for small  $St_f$ , but this trend reverses smoothly at higher values of  $St_f$ . The large-scale clustering due to turbophoresis has also been observed in the DNS of turbulent channel flows<sup>15</sup> and in various experimental studies.<sup>16,17</sup>

Another example of the large-scale clustering of inertial particles is the phenomenon of turbulent thermal diffusion that is a combined effect of the temperature stratified turbulence and inertia of small particles.<sup>18,19</sup> Turbulent thermal diffusion is a purely collective phenomenon occurring in temperature stratified turbulence and resulting in the appearance of a non-zero large-scale effective pumping velocity of particles in the direction opposite to the mean temperature gradient. This implies that this phenomenon causes a non-diffusive turbulent flux of particles in the direction of the turbulent heat flux. A competition between the turbulent thermal diffusion and the turbulent diffusion determines the conditions for the formation of large-scale particle concentrations in the vicinity of the mean temperature minimum.

Turbulent thermal diffusion has been intensively investigated analytically<sup>18–25</sup> using different theoretical approaches. This effect has been detected in DNS,<sup>26,27</sup> Turbulent thermal diffusion has been observed in geophysical turbulence, e.g., in the atmosphere of the Earth<sup>28</sup> and the atmosphere of Titan,<sup>29</sup> and it has also been discussed in astrophysical turbulence applications.<sup>30</sup> Moreover, the phenomenon of turbulent thermal diffusion has been detected in laboratory experiments in nearly isotropic and homogeneous turbulence produced by two oscillating grids<sup>25,31–33</sup> and in a multi-fan produced turbulence.<sup>34</sup> Recently, the phenomenon of turbulent thermal diffusion has been found in an inhomogeneous and anisotropic stably stratified turbulence produced by one oscillating grid in the air flow.<sup>35</sup> These experiments have demonstrated the formation of inhomogeneous distributions of micrometer-size particles in the vicinity of the mean temperature minimum.

The main goal of the present study is to investigate experimentally the phenomenon of turbulent thermal diffusion of the micrometer-size solid particles in an inhomogeneous convective turbulence forced by a one oscillating grid in the air flow. In the experiments, we measure velocity fields applying particle image velocimetry (PIV). We measure the temperature field with a temperature probe equipped with 12 E thermocouples. In addition, we determine spatial distributions of small solid particles by a PIV system using the effect of the Mie light scattering by particles in the flow. We perform detailed comparisons of the obtained experimental results with those in the experiments in an inhomogeneous and anisotropic stably stratified turbulence produced by a one oscillating grid<sup>35</sup> and in a convective turbulence forced by two oscillating grids in the air flow.<sup>36</sup> This paper is organized as follows. In Sec. II, we elucidate the mechanism of the phenomenon of turbulent thermal diffusion and determine the turbulent flux of particles using the spectral  $\tau$  approach for the fully developed temperature-stratified turbulence. In Sec. III, we discuss our experimental facilities and instrumentation, and in Sec. IV, we describe the obtained experimental results. Finally, in Sec. V, we outline conclusions. In Appendix, we derive the expression for the particle turbulent flux for small Péclet numbers.

## II. TURBULENT THERMAL DIFFUSION

In this section, we determine the turbulent flux of particles in a temperature-stratified turbulence and elucidate the mechanism related to the effect of turbulent thermal diffusion. We study dynamics of small non-inertial particles advected by a turbulent fluid flow. An evolution of the particle number density  $n(t, \mathbf{x})$  in a fluid velocity field  $\mathbf{U}(t, \mathbf{x})$  is determined by the convective-diffusion equation as follows:

$$\frac{\partial n}{\partial t} + \nabla \cdot (n \mathbf{U} - D \nabla n) = 0, \quad (2)$$

where  $D = k_B T / (6\pi\rho\nu a_p)$  is the coefficient of the molecular (Brownian) diffusion of particles having the radius  $a_p$ . Here,  $T$  and  $\rho$  are the fluid temperature and density, respectively, and  $k_B$  is the Boltzmann constant. The fluid velocity is a turbulent field produced by, e.g., an external steering force. Equation (2) is a conservation law for the total number of particles that implies that the total number of particles is conserved in a closed volume. Here, we do not consider a coagulation of particles or chemical reactions as well as condensation or evaporation of droplets, which change the total number of particles or droplets in a closed volume.

Assuming for simplicity that the diffusion coefficient is independent of coordinates, Eq. (2) can be rewritten as

$$\frac{\partial n}{\partial t} + \nabla \cdot (n \mathbf{U}) = D \Delta n. \quad (3)$$

We use a point-particle approximation that implies that the size of particles is very small in comparison with all possible scales of fluid motions. When the fluid velocity is much less than the sound speed (i.e., for low-Mach-number fluid flows), the continuity equation for the fluid density can be used in an anelastic approximation,  $\nabla \cdot (\rho \mathbf{U}) = 0$ . This equation can be rewritten as  $\nabla \cdot \mathbf{U} = -(\mathbf{U} \cdot \nabla) \ln \rho$ , i.e., the anelastic approximation takes into account an inhomogeneous fluid density.

We study a long-term evolution of the particle number density in spatial scales  $L_n$ , which are much larger than the integral scale of turbulence  $\ell_0$ , and during the time scales  $t_m$ , which are much larger than the turbulent time scales  $\tau_0$ . We use a mean-field approach in which all quantities are decomposed into the mean and fluctuating parts, where the fluctuating parts have zero mean values, i.e., we use the Reynolds averaging. In particular, the particle number density  $n = \bar{n} + n'$ , where  $\bar{n} = \langle n \rangle$  is the mean particle number density and  $n'$  are the particle number density fluctuations and  $\langle n' \rangle = 0$ . The angular brackets  $\langle \dots \rangle$  denote an ensemble averaging. Averaging Eq. (3) over an ensemble of a turbulent velocity field, we arrive at the mean-field equation for the particle number density as follows:

$$\frac{\partial \bar{n}}{\partial t} + \nabla \cdot (\bar{\mathbf{U}} \bar{n} + \langle \mathbf{u} n' \rangle) = D \Delta \bar{n}, \quad (4)$$

where  $\mathbf{F} \equiv \langle \mathbf{u} n' \rangle$  is the turbulent flux of particles. We consider for simplicity the case  $\bar{\mathbf{U}} = 0$ .

To derive an expression for the turbulent flux of particles, we obtain the equation for particle number density fluctuations  $n'$  by subtracting Eq. (4) from Eq. (3), which yields

$$\frac{\partial n'}{\partial t} = -\tilde{Q} - (\mathbf{u} \cdot \nabla) \bar{n} - \bar{n} (\nabla \cdot \mathbf{u}) + D \Delta n', \quad (5)$$

where  $\tilde{Q} = \nabla \cdot (n' \mathbf{u} - \langle n' \mathbf{u} \rangle)$  is the nonlinear term. The source term for particle number density fluctuations,  $-(\mathbf{u} \cdot \nabla) \bar{n}$ , results in the production of particle number density fluctuations by the tangling of the gradient  $\nabla \bar{n}$  of the mean particle number density by velocity fluctuations. The other source term,  $-\bar{n}(\nabla \cdot \mathbf{u})$ , for particle number density fluctuations can be rewritten as  $-\bar{n}(\nabla \cdot \mathbf{u}) = (\bar{n}/\bar{\rho})(\mathbf{u} \cdot \nabla)\bar{\rho}$ , where we take into account the anelastic approximation,  $\nabla \cdot \mathbf{u} = -(1/\bar{\rho})(\mathbf{u} \cdot \nabla)\bar{\rho}$ , which is also valid for the mean fluid density,  $\bar{\rho}$ . This implies that this source term describes a production of particle number density fluctuations by the tangling of the gradient  $\nabla \bar{\rho}$  of the mean fluid density by velocity fluctuations. We use the Péclet number  $Pe = |\tilde{Q}|/|D\Delta n'|$  defined as the dimensionless ratio of the absolute values of the nonlinear term  $|\tilde{Q}|$  to the diffusion term  $|D\Delta n'|$ . The Péclet number can be estimated as  $Pe = \ell_0 u_{rms}/D$ . Since the nonlinear equation (5) cannot be solved exactly for arbitrary Péclet numbers, we consider the case of large Péclet and Reynolds numbers, which corresponds to our laboratory experiments.

We apply the Fourier transform only in a  $\mathbf{k}$  space but not in a  $\omega$  space because in a fully developed Kolmogorov-like turbulence, the turbulent time is universally related to spatial scales. We take into account the nonlinear terms in equations for velocity and particle number density fluctuations and apply the spectral  $\tau$  approach<sup>37,38</sup> (see also Ref. 7 for a detailed discussion).

For simplicity, we consider a one-way coupling by taking into account the effect of turbulence on the particle number density and neglecting the feedback effect of the particle number density on the turbulent fluid flow. The one-way coupling approximation is valid when the spatial density of particles  $n m_p$  is much smaller than the fluid density  $\rho$ , where  $m_p$  is the particle mass. First, we consider non-inertial particles, which means that the particles move with the fluid velocity, i.e., the particle number density is a passive scalar.

We use a multi-scale approach,<sup>39</sup> i.e., we consider the one-point second-order correlation function as

$$\begin{aligned} \langle u_i(t, \mathbf{x}) n'(t, \mathbf{x}) \rangle &\equiv \lim_{\mathbf{x} \rightarrow \mathbf{y}} \langle u_i(t, \mathbf{x}) n'(t, \mathbf{y}) \rangle \\ &= \lim_{\mathbf{r} \rightarrow 0} \int F_i(t, \mathbf{k}, \mathbf{R}) \exp(i\mathbf{k} \cdot \mathbf{r}) d\mathbf{k} = \int F_i(t, \mathbf{k}, \mathbf{R}) d\mathbf{k}, \end{aligned} \quad (6)$$

where  $F_i(t, \mathbf{k}, \mathbf{R}) = \int F_i(t, \mathbf{k}, \mathbf{K}) \exp(i\mathbf{K} \cdot \mathbf{R}) d\mathbf{K}$  and  $F_i(t, \mathbf{k}, \mathbf{K}) = \langle u_i(t, \mathbf{k} + \mathbf{K}/2) n'(t, -\mathbf{k} + \mathbf{K}/2) \rangle$ . Here, the mean fields depend on “slow” variables  $\mathbf{R} = (\mathbf{x} + \mathbf{y})/2$ , while fluctuations depend on “fast” variables  $\mathbf{r} = \mathbf{x} - \mathbf{y}$ , which correspond to large-scale and small-scale spatial variables, respectively. In the Fourier space,  $\mathbf{k} = (\mathbf{k}_1 - \mathbf{k}_2)/2$  corresponds to the small scales, and  $\mathbf{K} = \mathbf{k}_1 + \mathbf{k}_2$  characterizes the large scales, where we use the Fourier transform,  $u_i(t, \mathbf{x}) = \int u_i(t, \mathbf{k}_1) \exp(i\mathbf{k}_1 \cdot \mathbf{x}) d\mathbf{k}_1$ . For homogeneous turbulence, the correlation function,  $F_i(t, \mathbf{k}, \mathbf{R})$ , is independent of the large-scale variable  $\mathbf{R}$ , i.e.,  $F_i(t, \mathbf{k}, \mathbf{R}) = F_i(t, \mathbf{k})$ .

To obtain expression for the particle turbulent flux, we use Eq. (5) written in a Fourier space. This allows us to derive the equation for the correlation function  $F_j(t, \mathbf{k})$  in a Fourier space as

$$\frac{\partial F_j(\mathbf{k})}{\partial t} = -(\nabla_i \bar{n} - i k_i \bar{n}) f_{ij}(-\mathbf{k}) + \hat{\mathcal{M}} F_j^{(III)}(\mathbf{k}), \quad (7)$$

where for the brevity of notation, hereafter we omit argument  $t$  in the correlation functions. Here,  $\hat{\mathcal{M}} F_j^{(III)}(\mathbf{k}) = \langle [\partial u_i(t, \mathbf{k}) / \partial t] n'(t, -\mathbf{k}) \rangle$

$-\langle u_i(t, \mathbf{k}) Q(t, -\mathbf{k}) \rangle$  are the third-order moments appearing due to the nonlinear terms  $\tilde{Q}$  in Eq. (5) and the nonlinear Navier–Stokes equation. Here,  $f_{ij}(\mathbf{k}) = \langle u_i(t, \mathbf{k}) u_j(t, -\mathbf{k}) \rangle$  and  $Q = \tilde{Q} - D\Delta n'$ .

We use the spectral  $\tau$  approximation.<sup>37,38</sup> This approximation postulates that the deviations of the third-moment terms,  $\hat{\mathcal{M}} F_j^{(III)}(\mathbf{k})$ , from the contributions to these terms afforded by the background turbulence,  $\hat{\mathcal{M}} F_j^{(III,0)}(\mathbf{k})$ , can be expressed through the similar deviations of the second moments,  $F(\mathbf{k}) - F^{(0)}(\mathbf{k})$ , as follows:

$$\hat{\mathcal{M}} F_j^{(III)}(\mathbf{k}) - \hat{\mathcal{M}} F_j^{(III,0)}(\mathbf{k}) = -\frac{1}{\tau_r(k)} [F(\mathbf{k}) - F^{(0)}(\mathbf{k})], \quad (8)$$

where  $\tau_r(k)$  is the scale-dependent relaxation time, which can be identified with the correlation time  $\tau(k)$  of the turbulent velocity field for large Reynolds and Péclet numbers. The functions with the superscript (0) correspond to the background turbulence with a zero turbulent particle flux and a zero level of particle number density fluctuations.

Consequently, Eq. (8) reduces to  $\hat{\mathcal{M}} F_j^{(III)}(\mathbf{k}) = -F_j(\mathbf{k})/\tau(k)$ . Validation of the  $\tau$  approximation for different situations has been performed in various numerical simulations<sup>26,27,40–44</sup> (see also Ref. 7 for a detailed discussion of the ranges of applicability of this approach).

We assume that the characteristic time of variation of the second moment  $F_i(\mathbf{k})$  is substantially larger than the correlation time  $\tau(k)$  for all turbulence scales. This allows us to use a steady-state solution of Eq. (7). Applying the spectral  $\tau$  approximation and using the steady-state solution of Eq. (7), we obtain the following formula for the turbulent flux of particles,  $F_j(\mathbf{k})$ , as

$$F_j(\mathbf{k}) = -\tau(k) (\nabla_i \bar{n} - i k_i \bar{n}) f_{ij}^{(0)}(-\mathbf{k}), \quad (9)$$

where since we consider a one-way coupling, we replace the function  $f_{ij}(\mathbf{k})$  by  $f_{ij}^{(0)}(\mathbf{k})$  in Eq. (9).

We use the following model for the second moments of the turbulent velocity field  $f_{ij}^{(0)}(\mathbf{k}) \equiv \langle u_i(\mathbf{k}) u_j(-\mathbf{k}) \rangle^{(0)}$  of an isotropic and homogeneous background turbulence in the anelastic approximation in a Fourier space:

$$f_{ij}^{(0)}(\mathbf{k}) = \frac{\langle \mathbf{u}^2 \rangle E(k)}{8\pi k^2} \left[ \delta_{ij} - k_{ij} + \frac{i}{k^2} (\lambda_i k_j - \lambda_j k_i) \right], \quad (10)$$

where  $k_{ij} = k_i k_j / k^2$ ,  $\delta_{ij}$  is the Kronecker unit tensor,  $\boldsymbol{\lambda} = -(\nabla \bar{\rho}) / \bar{\rho}$ , the spectrum function of the turbulent kinetic energy density is  $E(k) = (2/3) k_0^{-1} (k/k_0)^{-5/3}$  [see Ref. 7 for a detailed derivation of Eq. (10)]. Here, the wavenumber  $k$  varies within the interval  $k_0 \leq k \leq k_\nu$  corresponding to the inertial range of scales, the wave number  $k_0 = 1/\ell_0$ , the length  $\ell_0$  is the integral scale of turbulence, the wave number  $k_\nu = \ell_\nu^{-1}$ , where  $\ell_\nu = \ell_0 Re^{-3/4}$  is the Kolmogorov (viscous) scale and the turbulent correlation time is given by  $\tau(k) = 2\tau_0 (k/k_0)^{-2/3}$ , where  $\tau_0$  is the characteristic turbulent time. The functions  $E(k)$  and  $\tau(k)$  correspond to the fully developed turbulence with the Kolmogorov scalings.

Using Eqs. (6), (9), and (10), we determine the turbulent flux of particles  $F_i = \langle u_i n' \rangle$  as follows:

$$\begin{aligned} F_i &= -\frac{\langle \mathbf{u}^2 \rangle}{8\pi} \int_{k_0}^{k_\nu} \tau(k) E(k) dk \int_0^{2\pi} d\varphi \int_0^\pi \sin \vartheta d\vartheta \\ &\quad \times [(\delta_{ij} - k_{ij}) \nabla_i \bar{n} + (\lambda_j - \lambda_i k_{ij}) \bar{n}]. \end{aligned} \quad (11)$$

For the integration over  $\mathbf{k}$  in Eq. (11), we use the integrals given by  $\int_0^{2\pi} d\varphi \int_0^\pi \sin \vartheta d\vartheta k_{ij} = (4\pi/3) \delta_{ij}$  and  $\int_{k_0}^{k_\infty} \tau(k) E(k) dk = \tau_0$ . After integration over  $\mathbf{k}$ , we obtain the particle turbulent flux  $\langle n' \mathbf{u} \rangle$  as

$$\langle n' \mathbf{u} \rangle = \mathbf{V}^{\text{eff}} \bar{n} - D_T \nabla \bar{n}, \quad (12)$$

where the turbulent diffusion coefficient is

$$D_T = \frac{1}{3} \tau_0 \langle \mathbf{u}^2 \rangle \quad (13)$$

and the effective pumping velocity is given by

$$\mathbf{V}^{\text{eff}} = -D_T \lambda = D_T \frac{\nabla \bar{P}}{\bar{P}}. \quad (14)$$

Equations (12)–(14) are in agreement with those obtained using the dimensional analysis (see Ref. 7 for detailed discussions). Remarkably, the phenomenon of the turbulent diffusion of particles was predicted more than 100 years ago in Ref. 45.

Note that for small Péclet numbers, Eqs. (12) and (14) are also valid, but the turbulent diffusion coefficient in these equations should be replaced by  $D_T = [(q-1)/3(q+1)] \tau_0 \langle \mathbf{u}^2 \rangle \text{Pe}$  (see the Appendix). Here,  $q$  is the exponent of the spectra of the turbulent kinetic energy. For small Péclet numbers, the effect of interactions between turbulent diffusion and molecular diffusion for the mean particle number density can also be important.<sup>21,46</sup>

To understand the mechanism related to the effective pumping velocity  $\mathbf{V}^{\text{eff}}$ , we use the equation of state for a perfect gas

$$P = \frac{k_B}{m_\mu} \rho T \equiv \frac{R}{\mu} \rho T, \quad (15)$$

where  $P$  is the fluid pressure,  $k_B = R/N_A$  is the Boltzmann constant,  $R$  is the gas constant,  $N_A$  is the Avogadro number,  $\mu = m_\mu N_A$  is the molar mass, and  $m_\mu$  is the molecular mass. We rewrite the equation of state for the mean fields assuming that  $\bar{P} \bar{T} \gg \langle \rho' \theta' \rangle$ , where  $\rho'$  and  $\theta'$  are the fluctuations of the fluid density and temperature, respectively, and  $\bar{T}$  is the mean fluid temperature. Thus, the equation of state for the mean fields reads

$$\bar{P} = \frac{k_B}{m_\mu} \bar{\rho} \bar{T}, \quad (16)$$

where  $\bar{P}$  is the mean pressure.

Using Eq. (16), we express the gradient of the mean fluid density in terms of the gradients of the mean fluid pressure  $\nabla \bar{P}$  and mean fluid temperature  $\nabla \bar{T}$  as

$$\frac{\nabla \bar{\rho}}{\bar{\rho}} = \frac{\nabla \bar{P}}{\bar{P}} - \frac{\nabla \bar{T}}{\bar{T}}. \quad (17)$$

Substituting Eq. (17) into Eq. (14), we obtain the final expression for the effective pumping velocity of non-inertial particles as

$$\mathbf{V}^{\text{eff}} = D_T \left( \frac{\nabla \bar{P}}{\bar{P}} - \frac{\nabla \bar{T}}{\bar{T}} \right). \quad (18)$$

To understand different terms in Eq. (18), we compare the molecular and turbulent fluxes of particles (or gaseous admixtures). The equation for the number density of particles reads

$$\frac{\partial n}{\partial t} + \nabla \cdot (n \mathbf{U}) = -\nabla \cdot \mathbf{F}_M, \quad (19)$$

where the molecular flux of particles  $\mathbf{F}_M$  is given by

$$\mathbf{F}_M = -D \left( \nabla n + k_t \frac{\nabla T}{T} + k_p \frac{\nabla P}{P} \right), \quad (20)$$

which comprises three terms: molecular diffusion ( $\propto \nabla n$ ), molecular thermal diffusion for gases or thermophoresis for particles ( $\propto k_t \nabla T$ ), and molecular barodiffusion ( $\propto k_p \nabla P$ ), where  $k_t$  is the molecular thermal diffusion ratio and  $k_p$  is the molecular barodiffusion ratio. Note that the phenomenon of molecular thermal diffusion in gases has been predicted long ago in Refs. 47–49.

In turbulent flows, the turbulent flux of particles can be rewritten as

$$\mathbf{F}_T \equiv \langle n' \mathbf{u} \rangle = -D_T \left( \nabla \bar{n} + \bar{n} \frac{\nabla \bar{T}}{\bar{T}} - \bar{n} \frac{\nabla \bar{P}}{\bar{P}} \right), \quad (21)$$

which is obtained by the substitution of Eq. (18) to Eq. (12). Comparing the molecular flux of particles (20) and the turbulent flux of particles (21), we can interpret the new additional turbulent fluxes as fluxes caused by the effects of turbulent thermal diffusion [ $\propto k_T (\nabla \bar{T})/\bar{T}$ ] and turbulent barodiffusion [ $\propto k_P (\nabla \bar{P})/\bar{P}$ ], where

$$\mathbf{F}_T \equiv \langle n' \mathbf{u} \rangle = -D_T \left( \nabla \bar{n} + k_T \frac{\nabla \bar{T}}{\bar{T}} + k_P \frac{\nabla \bar{P}}{\bar{P}} \right) \quad (22)$$

and  $k_T = \bar{n}$  is the turbulent thermal diffusion ratio and  $k_P = -\bar{n}$  is the turbulent barodiffusion ratio. These phenomena have been predicted in Refs. 18 and 19.

For small inertial particles, the expression for the effective pumping velocity reads<sup>11</sup> (see also Ref. 7 for a detailed derivation)

$$\mathbf{V}^{\text{eff}} = -\alpha D_T \nabla \ln \bar{T}, \quad (23)$$

where

$$\alpha = 1 + 2 \frac{m_p}{m_\mu} \left( \frac{\ln \text{Re}}{\text{Pe}} \right) \frac{\bar{T}}{\bar{T}_*} = 1 + 2 \frac{V_g L_p \ln \text{Re}}{u_0 \ell_0}, \quad (24)$$

where  $\tau_p V_T^2 = \gamma (m_p/m_\mu) D = \gamma V_g L_p \bar{T}_*/\bar{T}$ . Here,  $\gamma = c_p/c_v$  is the ratio of specific heats,  $V_T = (\gamma k_B \bar{T}_*/m_\mu)^{1/2}$  is the thermal velocity,  $\bar{T}_*$  is the characteristic mean fluid temperature, and  $L_p = |\nabla_z \bar{P}/\bar{P}|^{-1}$  is the pressure height scale. In derivation of Eq. (24), we take into account that the Stokes time can be written as  $\tau_p = \bar{\rho} V_g L_p / \bar{P}$  with  $V_g = \tau_p \mathbf{g}$  being the terminal fall velocity of particles, where  $\mathbf{g}$  is the acceleration caused by the gravity field. For large Péclet numbers,  $\text{Pe} \gg 1$ , the turbulent thermal diffusion coefficient  $\alpha = 1$  for non-inertial particles, while for inertial particles,  $\alpha$  depends on the particle mass, the Reynolds, and Péclet numbers.

The non-diffusive turbulent flux of particles,  $\bar{n} \mathbf{V}^{\text{eff}}$ , toward the mean temperature minimum is the main reason for the formation of large-scale inhomogeneous distributions of inertial particles in temperature-stratified turbulence. The steady-state solution of the equation for the mean number density of inertial particles,

$$\frac{\partial \bar{n}}{\partial t} + \nabla \cdot \left[ \bar{n} (\mathbf{V}_g + \mathbf{V}^{\text{eff}}) - (D + D_T) \nabla \bar{n} \right] = 0, \quad (25)$$



satisfying the boundary condition with a zero total particle flux at the boundary, is given by

$$\frac{\bar{n}}{\bar{n}_b} = \left( \frac{\bar{T}}{\bar{T}_b} \right)^{-\frac{\alpha D_T}{D+D_T}} \exp \left[ - \int_{z_b}^z \frac{V_g}{D+D_T} dz' \right], \quad (26)$$

where the subscripts (b) represent the values of the mean temperature and the mean particle number density at the boundary  $z = z_b$ . Equation (26) implies that small inertial particles are accumulated below the mean temperature minimum due to the gravity field.

The mechanism for the turbulent thermal diffusion for inertial particles is as follows. Particles inside the turbulent eddies due to its inertia tend to be drift out to the boundary regions between the eddies due to the centrifugal inertial force. Indeed, for large Péclet numbers, the molecular diffusion of particles in equation for the number density of inertial particles

$$\frac{\partial n}{\partial t} + \nabla \cdot (n \mathbf{u}^{(p)} - D \nabla n) = 0 \quad (27)$$

can be neglected, so that

$$\nabla \cdot \mathbf{u}^{(p)} \approx -n^{-1} \left[ \frac{\partial n}{\partial t} + (\mathbf{u}^{(p)} \cdot \nabla) n \right] \equiv -n^{-1} \frac{dn}{dt}, \quad (28)$$

where  $\mathbf{u}^{(p)}$  is the particle velocity. On the other hand, for inertial particles,  $\nabla \cdot \mathbf{u}^{(p)} = \nabla \cdot \mathbf{u} + (\tau_p/\bar{\rho}) \nabla^2 p$ . Indeed, the solution of the equation of motion for inertial particles,

$$\frac{d\mathbf{u}^{(p)}}{dt} = -\frac{\mathbf{u}^{(p)} - \mathbf{u}}{\tau_p} + \mathbf{g}, \quad (29)$$

for  $\rho_p \gg \bar{\rho}$  and small Stokes time, reads<sup>50</sup>  $\mathbf{u}^{(p)} = \mathbf{u} - \tau_p (d\mathbf{u}/dt) + \tau_p \mathbf{g} + O(\tau_p^2) \approx \mathbf{u} + \tau_p (\nabla p/\bar{\rho}) + \tau_p \mathbf{g} + O(\tau_p^2)$ . Here,  $\rho_p$  is the material density of particles. This yields the equation for  $\nabla \cdot \mathbf{u}^{(p)}$ . Therefore, in regions with maximum fluid pressure fluctuations (where  $\nabla^2 p < 0$ ), there is accumulation of inertial particles, i.e.,  $dn'/dt \propto -\bar{n} (\tau_p/\bar{\rho}) \nabla^2 p > 0$ . These regions obey low vorticity and high strain rate. Similarly, there is an outflow of inertial particles from regions with minimum fluid pressure.

In a homogeneous and isotropic turbulence with a zero gradient of the mean temperature, there is no preferential direction. This implies that in a homogeneous and isotropic turbulence, there is no large-scale effect of particle accumulation, and the pressure (temperature) of the surrounding fluid is not correlated with the turbulent velocity field. The only non-zero correlation is  $\langle (\mathbf{u} \cdot \nabla) p \rangle$ , which contributes to the flux of the turbulent kinetic energy density.

In a temperature-stratified turbulence, the turbulent heat flux does not vanish, so that fluctuations of fluid temperature  $\theta$  and velocity  $\mathbf{u}$  are correlated, i.e.,  $\langle \theta \mathbf{u} \rangle \neq 0$ . Fluctuations of the temperature result in pressure fluctuations, which cause fluctuations of the particle number density. Increase of the pressure of the surrounding fluid is accompanied by an accumulation of particles, and the direction of the turbulent flux of particles coincides with that of the turbulent heat flux. The turbulent flux of particles is directed toward the minimum of the mean temperature. This causes the formation of large-scale inhomogeneous structures in the spatial distribution of inertial particles in the vicinity of the mean temperature minimum. In the next sections,

we will study this phenomenon in the experiments with a forced convective turbulence.

### III. EXPERIMENTAL SETUP

In this section, we describe the experimental setup and measurement technique. We investigate the turbulent thermal diffusion of small solid particles in experiments with a convective turbulence forced by a one oscillating grid in the air flow. We conduct experiments in a rectangular transparent chamber with dimensions  $L_x \times L_y \times L_z$  with  $L_x = L_z = 26$  cm and  $L_y = 53$  cm, where  $Z$  is along the vertical direction and  $Y$  is perpendicular to the grid plain. The oscillating grid with bars arranged in a square array is parallel to the side walls of the chamber; it is positioned at a distance of two grid meshes from the left sidewall of the chamber (see Fig. 1).

Two aluminum heat exchangers with rectangular pins  $3 \times 3 \times 15$  mm are attached to the bottom (heated) and top (cooled) walls of the chamber, which allow one to form a large vertical mean temperature gradient of up to 1.8 K/cm in the main fluid flow and about 7 K/cm close to the walls. We measure the temperature field using a temperature probe equipped with 12 E-thermocouples. The thermocouples with a diameter of 0.13 mm and a sensitivity of  $\approx 75 \mu V/K$  are attached to a vertical rod with a diameter of 4 mm, and the mean distance between thermocouples is about 21.6 mm (see for details, Ref. 35). We measure the temperature field in many locations. The data are recorded using the developed software based on LabView 7.0, and the temperature maps are obtained using Matlab 9.7.0.

We measure the velocity field with a particle image velocimetry (PIV) system,<sup>51–53</sup> consisting of a Nd-YAG laser (Continuum Surelite  $2 \times 170$  mJ) and a progressive-scan 12 bit digital CCD camera (with pixel size  $6.45 \times 6.45 \mu m^2$  and  $1376 \times 1040$  pixels). As a tracer for the PIV measurements, we use an incense smoke with spherical solid particles having a mean diameter of  $0.7 \mu m$  and the material density  $\rho_p \approx 10^3 \rho$ . The particles are produced by high temperature sublimation of solid incense grains (see for details Ref. 35).

For instance, the velocity fields in our experiments have been measured in a flow domain  $209.09 \times 155.43$  mm<sup>2</sup> with a spatial resolution of  $1376 \times 1024$  pixels, so that a spatial resolution of  $151 \mu m/\text{pixel}$  has been achieved. We analyze the velocity field in the probed region with interrogation windows of  $16 \times 16$  pixels. Using the velocity measurements, various turbulence characteristics [e.g., the mean and the root mean square (r.m.s.) velocities, two-point

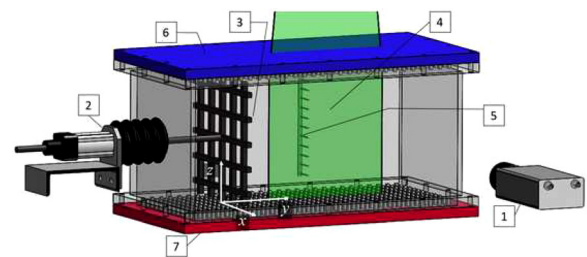


**FIG. 1.** Experimental setup with the forced convective turbulence: (1) digital CCD camera; (2) rod driven by the speed-controlled motor; (3) oscillating grid; (4) laser light sheet; (5) temperature probe equipped with 12 E-thermocouples; (6) heat exchanger at the top cooled wall of the chamber; and (7) heat exchanger at the bottom heated wall of the chamber.

correlation functions, and an integral scale of turbulence] have been obtained in our experiments. In particular, we determine the mean and r.m.s. velocities for every point of a velocity map by averaging over 530 independent maps. We also obtain the integral length scales of turbulences  $\ell_y$  and  $\ell_z$  in the horizontal  $Y$  and the vertical  $Z$  directions from the two-point correlation functions of the velocity field.

Next, we obtain the particle spatial distribution by the PIV system using the effect of the Mie light scattering by particles.<sup>54</sup> To this end, we determine the mean intensity of scattered light in  $80 \times 64$  interrogation windows with the size  $16 \times 16$  pixels. This allows us to find the vertical distribution of the intensity of the scattered light in 80 vertical strips composed of 64 interrogation windows. In particular, we take into account that the light radiation energy flux scattered by small particles is given by  $E_s \propto E_0 \Psi(\pi d_p / \lambda; a_0; n)$ . Here,  $\Psi$  is the scattering function,  $d_p$  is the particle diameter,  $\lambda$  is the wavelength, and  $a_0$  is the index of refraction. The energy flux incident at the particle is given by  $E_0 \propto \pi d_p^2 / 4$ . Note that when  $\lambda > \pi d_p$ , the scattering function  $\Psi$  is determined by Rayleigh's law,  $\Psi \propto d_p^4$ . In opposite case for small  $\lambda$ , the scattering function  $\Psi$  is independent of the particle diameter and the wavelength. In a general case, the scattering function  $\Psi$  is determined by the Mie equations.<sup>55</sup>

Finally, we take into account that the light radiation energy flux scattered by small particles is  $E_s \propto E_0 n (\pi d_p^2 / 4)$ . This implies that the scattered light energy flux incident on the charge-coupled device (CCD) camera probe is proportional to the particle number density  $n$ . The ratio of the scattered radiation fluxes at two locations in the flow and at the image measured with the CCD camera is equal to the ratio of the particle number densities at these two locations. For the normalization of the scattered light intensity  $E^T$  obtained in a temperature-stratified turbulence, we use the distribution of the scattered light intensity  $E$  measured in the isothermal case obtained under the same conditions. Indeed, as follows from our measurements applying different concentrations of the incense smoke, the distribution of the scattered light intensity averaged over a vertical coordinate is independent of the particle number density in the isothermal flow. Therefore, using this normalization, we can characterize the spatial distribution of particle number density  $n \propto E^T / E$  in the non-isothermal turbulence.

Note that the measurement technique and data processing procedure described in this section are similar to those used by us in various experiments with turbulent convection<sup>36,56,57</sup> and stably stratified turbulence.<sup>35,58</sup> In addition, the similar measurement technique and data processing procedure in the experiments have been performed previously by us to investigate the phenomenon of turbulent thermal diffusion in a homogeneous turbulence<sup>25,31–33</sup> as well as for the study of small-scale particle clustering.<sup>59</sup>

#### IV. EXPERIMENTAL RESULTS

In this section, we discuss the obtained experimental results in a forced convective turbulence with a one oscillating grid in the air flow. There are two sources of turbulence in a forced convective turbulence with a heated bottom wall of the chamber and the cooling upper wall. In particular, the turbulent kinetic energy is increased by buoyancy and the grid oscillations. In our experiments, the frequency  $f$  of the grid oscillations is  $f = 10.5$  Hz, which yields the maximum turbulence intensity in our experimental setup.

Note that early laboratory experiments,<sup>60–66</sup> which have been conducted in isothermal turbulence with a one oscillating grid in a

water flow, have demonstrated that the r.m.s. velocity behaves as  $\sqrt{\langle u^2 \rangle} \propto f Y^{-1}$ , while the integral turbulence length scale increases linearly with the distance  $Y$  from a grid. Therefore, the fluid Reynolds numbers and the turbulent diffusion coefficient of particles are nearly independent of the distance  $Y$  from the grid. Our previous<sup>35</sup> and present studies in turbulence with one oscillating grid confirm these findings.

In the present study, we conduct experiments in a forced convective turbulence with one oscillating grid for the temperature difference  $\Delta T = 50$  K between the bottom and top walls of the chamber. Using the PIV system, we measure the velocity field in the chamber for an isothermal and a forced convective turbulence, which allows us to determine various turbulence characteristics. In particular, we obtain the spatial distributions of the mean velocity in convective turbulence with large-scale circulations, the vertical and horizontal profiles of the r.m.s. turbulent velocity, and the integral turbulence length scales. Since the oscillating grid is located near by the left wall of the chamber, and the amplitude of the grid oscillations is 6 cm, we measure the velocity field in the horizontal direction starting 20 cm away from the left wall of the chamber. We compare these results with those obtained in our recent experiments<sup>35</sup> with stably stratified turbulence produced by one oscillating grid in the air flow.

Figure 2 with the mean velocity patterns  $\bar{U}$  in the main fluid flow for isothermal, stably stratified turbulence, and convective turbulence demonstrates that the temperature stratification and additional forcing strongly affect the mean velocity distributions. Contrary to our previous experiments with a forced convection with two oscillating grids,<sup>36</sup> the large-scale circulations in the convective turbulence with one oscillating grid are not destroyed at a frequency of 10.5 Hz of the grid oscillations, but their structure is strongly deformed (see the bottom panel in Fig. 2).

Similar effects of the temperature stratification and additional forcing are also seen in the horizontal profiles of velocity fluctuations (see Fig. 3, where we plot the horizontal  $u_y^{(rms)}$  and vertical  $u_z^{(rms)}$  components of turbulent velocities as the functions of  $Y$  averaged over the vertical coordinate  $Z$  for isothermal turbulence, stably stratified turbulence, and convective turbulence). The turbulent velocities for convective turbulence are larger than for isothermal turbulence, while the turbulent velocities for the stably stratified turbulence are smaller than those for isothermal and convective turbulence. This is because the buoyancy increases the turbulent kinetic energy for convective turbulence and decreases it for stably stratified turbulence.

The oscillating grid strongly affects convective turbulence, as can be seen in Figs. 4 and 5, where we show the distributions of the turbulent velocity  $u_{tot}^{(rms)} = [\langle u_y^2 \rangle + \langle u_z^2 \rangle]^{1/2}$  and the anisotropy parameter  $u_z^{(rms)} / u_y^{(rms)}$  for the turbulent velocity components for isothermal, stably stratified, and convective turbulence. Figure 5 demonstrates that the anisotropy for isothermal and stably stratified turbulence is more stronger than that for convective turbulence. This is not surprising since the large-scale circulation enhances the mixing in the convective turbulence, and it results in a decrease in the turbulence anisotropy parameter  $u_z^{(rms)} / u_y^{(rms)}$ . The same tendencies are also seen for the horizontal  $\ell_y$  and vertical  $\ell_z$  integral turbulent length scales shown in Fig. 6, as well as for the distributions of the anisotropy parameter  $\ell_z / \ell_y$  of the integral turbulent length scales (see Fig. 7).

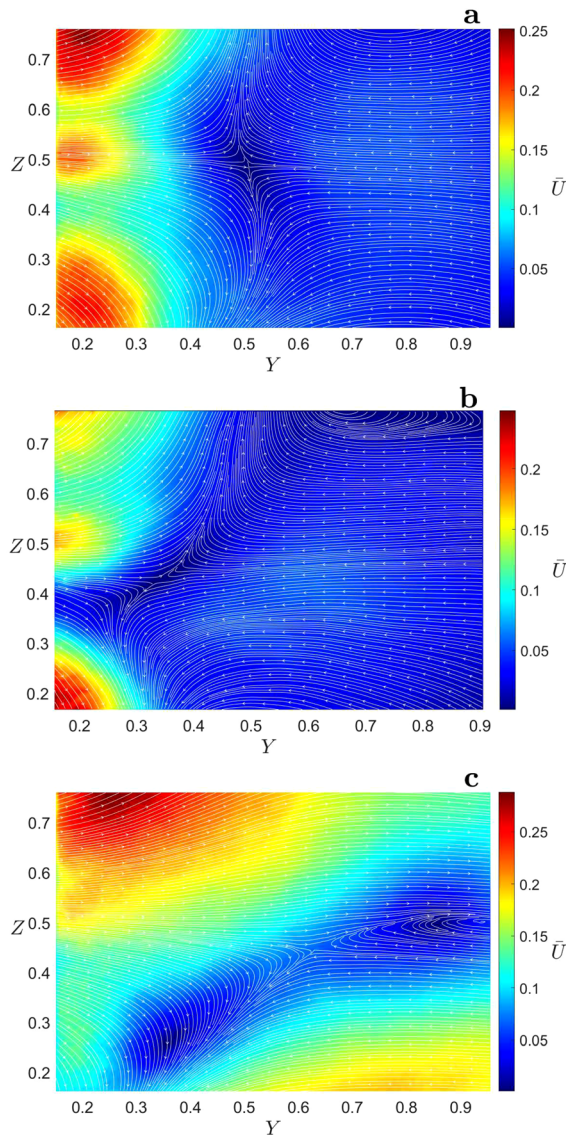


**FIG. 2.** Mean velocity field in the core flow for (a) isothermal turbulence; (b) stably stratified turbulence; and (c) forced convective turbulence. The velocity is measured in m/s, and coordinates  $Y$  and  $Z$  are normalized by  $L_z = 26$  cm.

To investigate the phenomenon of turbulent thermal diffusion in a forced convective turbulence, we measure the spatial distributions of the mean temperature and the mean particle number density. When small solid particles are injected into the chamber, their initial spatial distributions are nearly homogeneous. Due to the effective pumping velocity caused by a combined effect of temperature-stratified turbulence and particle inertia (described in terms of turbulent thermal diffusion), the final spatial distributions of the mean particle number density is expected to be strongly inhomogeneous.

Sedimentation of particles can also result in the formation of inhomogeneous particle distributions near the bottom wall of the chamber. However, this effect in our experiments is very weak because the terminal

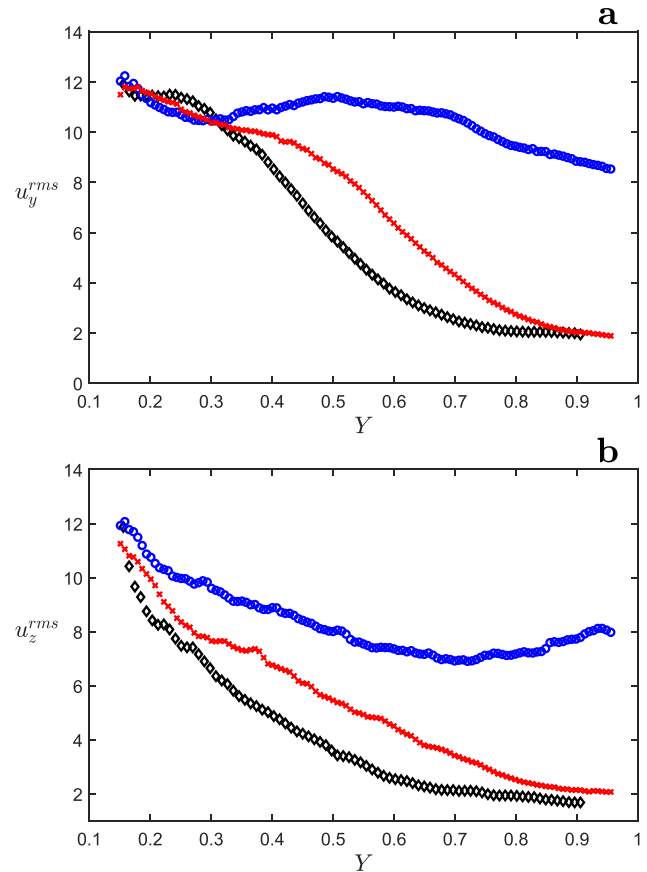


**FIG. 3.** Horizontal  $u_y^{(rms)}$  (a—upper panel) and vertical  $u_z^{(rms)}$  (b—lower panel) components of the turbulent velocity vs normalized coordinate  $Y$  averaged over the vertical coordinate  $Z$  for isothermal turbulence (red), stably stratified turbulence (black), and forced convective turbulence (blue). The velocity is measured in cm/s, and  $Y$  is normalized by  $L_z = 26$  cm.

fall velocity for the micrometer-size particles is about  $10^{-2}$  cm/s, while the turbulent velocity in the experiments with the forced convective turbulence is much larger than the particle terminal fall velocity (it is about 18 cm/s near the grid and is more than 12 cm/s far from the grid). On the other hand, our estimates for the effective pumping velocity due to turbulent thermal diffusion show that it is more than 3–5 cm/s near the grid and is about 0.5 cm/s far from the grid. Therefore, the turbulent velocity and the effective pumping velocity in our experiments are much larger than the terminal fall velocity for micrometer-size particles. Note also that the Stokes time for the micrometer-size particles is about  $1.5 \times 10^{-6}$  s, while the Kolmogorov time in the forced convective turbulence varies from  $7 \times 10^{-3}$  s near the grid up to  $4 \times 10^{-3}$  s far from the grid.

Our experiments with a forced convective turbulence with large-scale circulations show that the mean temperature is strongly nonuniform. In particular, as follows from Fig. 8 [where we plot vertical profiles of the relative normalized mean temperature  $(\bar{T} - \bar{T}_0)/\bar{T}_0$  averaged over different horizontal regions], the normalized mean temperature near the grid increases with the height  $Z$ , reaches the maximum, and decreases nearly linearly with the height  $Z$  (blue line), where  $\bar{T}_0$  is the reference mean temperature. Far from the grid, the



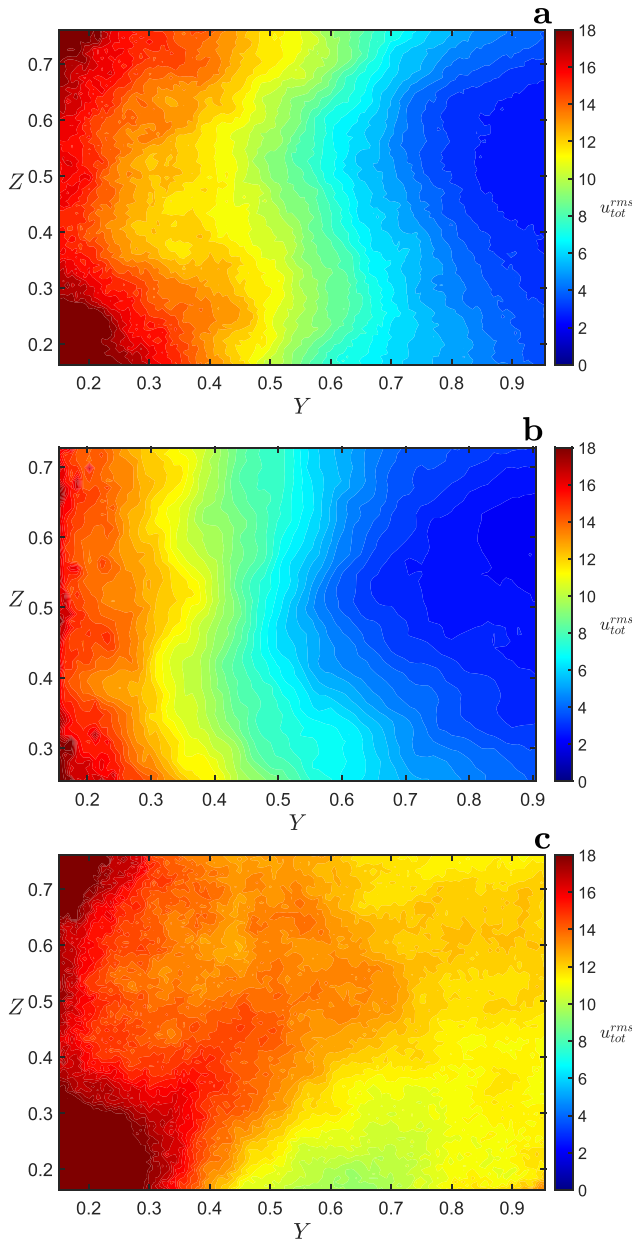


**FIG. 4.** Distributions of the turbulent velocity  $u_{\text{tot}}^{(\text{rms})} = [\langle u_y^2 \rangle + \langle u_z^2 \rangle]^{1/2}$  for (a) isothermal turbulence; (b) stably stratified turbulence; and (c) forced convective turbulence. The velocity is measured in cm/s, and coordinates are normalized by  $L_z = 26$  cm.

behavior of the mean temperature is even more complicated, e.g., the normalized mean temperature  $(\bar{T} - \bar{T}_0)/\bar{T}_0$  decreases with the height  $Z$ , reaches the minimum, and increases with the height  $Z$  reaching the maximum, and finally it decreases nearly linearly with the height  $Z$  (see red line in Fig. 8).

To demonstrate the phenomenon of turbulent thermal diffusion in the forced convective turbulence, we show in Figs. 9 and 10 the vertical profiles of the relative normalized mean temperature

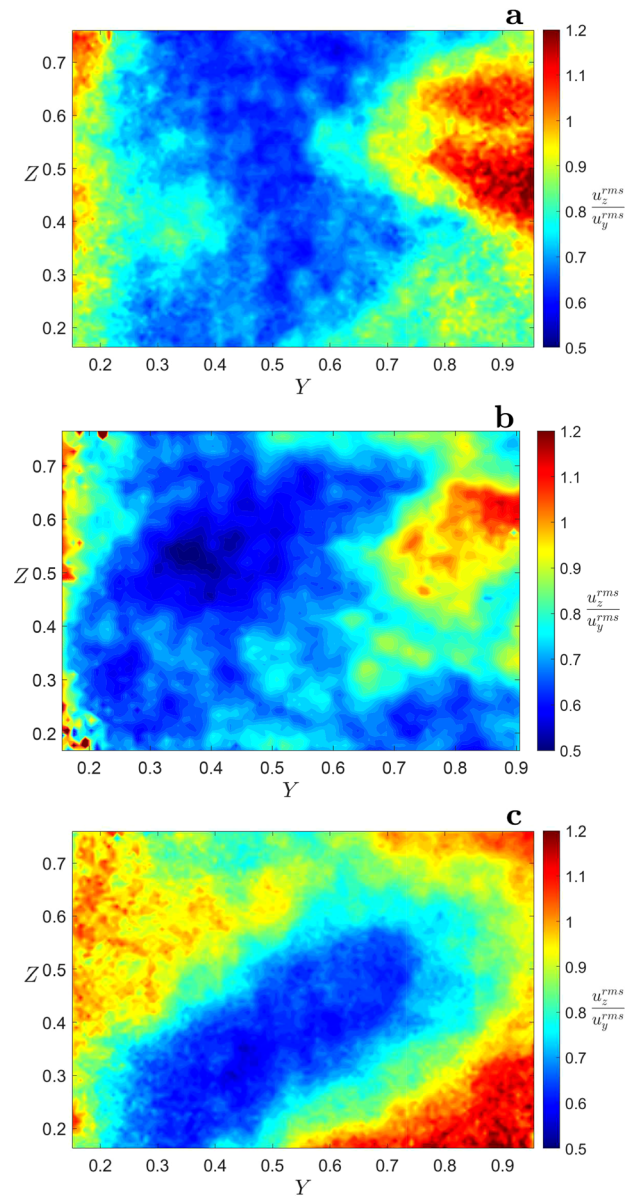


**FIG. 5.** Distributions of the anisotropy parameter  $u_z^{(\text{rms})}/u_y^{(\text{rms})}$  of the turbulent velocity for (a) isothermal turbulence; (b) stably stratified turbulence; and (c) forced convective turbulence. The velocity is measured in cm/s, and coordinates are normalized by  $L_z = 26$  cm.

$(\bar{T} - \bar{T}_0)/\bar{T}_0$  (black crosses) and the normalized mean particle number density  $\bar{n}(Y, Z)/\bar{n}_0$  (blue circles) near the grid (see Fig. 9) and far from the grid (see Fig. 10). Due to the phenomenon of turbulent thermal diffusion, the behavior of the normalized mean particle number density is opposite to the normalized mean temperature, i.e., the mean particle number density increases in the regions where the mean temperature decreases, and the mean particle number density reaches the maximum at the minimum of the mean temperature, and vice versa.

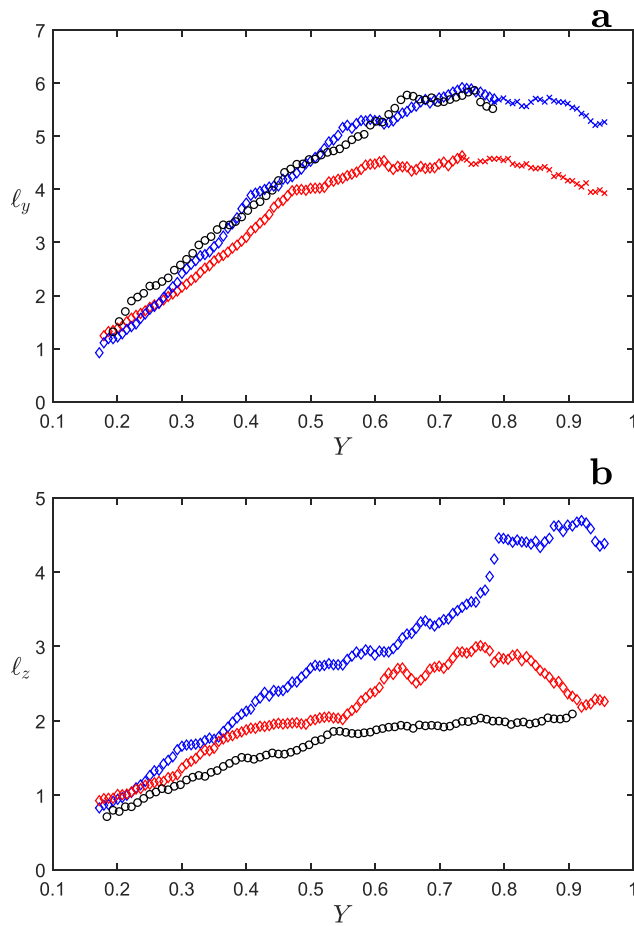


**FIG. 6.** Horizontal  $\ell_y$  (a—upper panel) and vertical  $\ell_z$  (b—lower panel) integral turbulent length scales vs normalized coordinate  $Y$  averaged over  $Z$  for isothermal turbulence (red); stably stratified turbulence (black); and forced convective turbulence (blue). The velocity is measured in cm/s, and  $Y$  is normalized by  $L_z = 26$  cm.

Therefore, Figs. 9 and 10 clearly demonstrate that particles are accumulated in the vicinity of the minimum of the mean temperature even in very complicated temperature field.

In the stably stratified turbulence, the behavior of the mean temperature and the mean particle number density is more simple than for the forced convective turbulence.<sup>35</sup> In particular, the mean temperature increases linearly with the height  $Z$  in the flow for the stably stratified turbulence, and the mean particle number density decreases linearly with the height  $Z$  due to the phenomenon of turbulent thermal diffusion.

To determine the effective turbulent thermal diffusion coefficient  $\alpha$  for particles in the forced inhomogeneous and anisotropic convective turbulence, we show in Fig. 11 the normalized mean particle number density  $\bar{n}/\bar{n}_0$  as a function of the relative normalized mean temperature  $(\bar{T} - \bar{T}_0)/\bar{T}_0$ , where the slope of this dependence yields the coefficient  $\alpha$ . In particular, we use a solution (26) for Eq. (25) for the mean particle number density  $\bar{n}$  obtained in a steady-state, where we assume that  $D_T \gg D$  and neglect small terminal fall velocity. Thus, we arrive at the following expression  $\bar{n}/\bar{n}_0 = 1 - \alpha(\bar{T} - \bar{T}_0)/\bar{T}_0$ , which shows that the effective turbulent thermal diffusion coefficient  $\alpha$  for particles in the

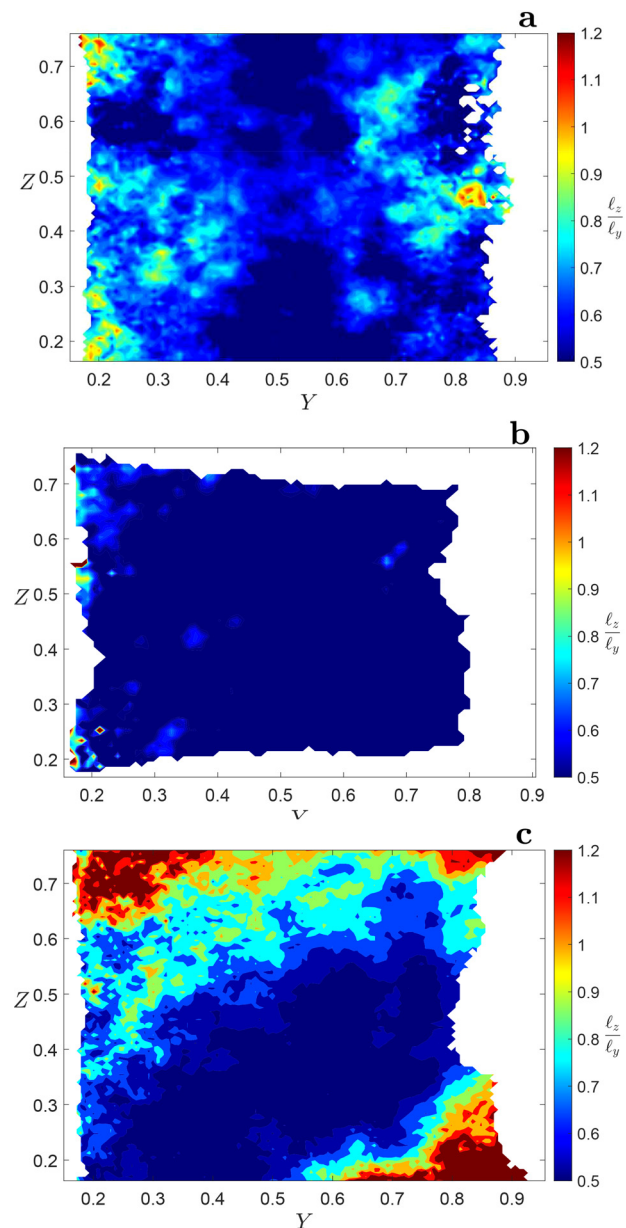


**FIG. 7.** Distributions of the anisotropy parameter  $\ell_z/\ell_y$  of the integral turbulent length scales for (a) isothermal turbulence; (b) stably stratified turbulence; and (c) forced convective turbulence. The velocity is measured in cm/s, and coordinates are normalized by  $L_z = 26$  cm.

forced convective turbulence is  $\alpha = 4.86$  for particles accumulated in the regions  $Y = 4\text{--}15$  cm and  $\alpha = 1.74$  for particles accumulated in the regions  $Y = 16\text{--}24$  cm (see Fig. 11). Now, we take into account that turbulence far from the grid is less stronger than that near the grid. This explains why the effective turbulent thermal diffusion coefficient  $\alpha$  near the grid is larger than that far from the grid. Therefore, this experimental study has demonstrated the effect of turbulent thermal diffusion in an inhomogeneous and anisotropic forced convective turbulence.

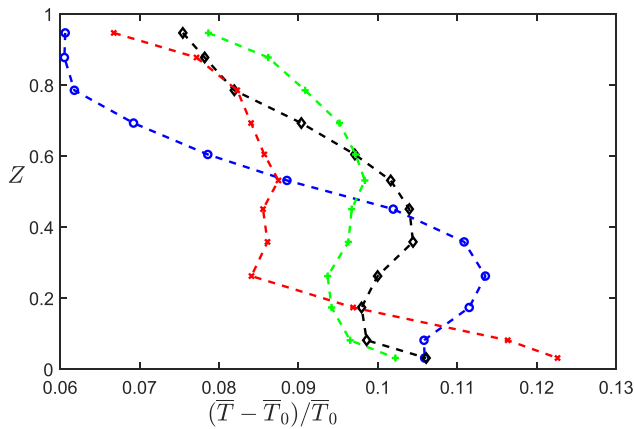


**FIG. 8.** Vertical profiles of the relative normalized mean temperature  $(\bar{T} - \bar{T}_0)/\bar{T}_0$  in the forced convective turbulence averaged over different horizontal regions:  $Y = 4-10$  cm (blue, circles);  $Y = 11-16$  cm (black, diamond);  $Y = 17-25$  cm (green, crosses); and  $Y = 24.5-28.5$  cm (red, slanting crosses), where  $Z$  is normalized by  $L_z = 26$  cm.

Note that since the Stokes numbers for the micrometer-size particles in our experiments with an inhomogeneous forced convective turbulence are very small [e.g.,  $St$  varies in the range  $(0.2-0.4) \times 10^{-3}$  depending on the distance from the grid], the turbophoresis effect is negligibly small.

## V. CONCLUSIONS

In the present study, the effect of the turbulent thermal diffusion of small solid particles, resulting in the formation of large-scale inhomogeneities in particle spatial distributions in a temperature-stratified turbulence, has been investigated experimentally for micrometer-size particles in an inhomogeneous convective turbulence forced by one oscillating grid in the air flow. The obtained experimental results have

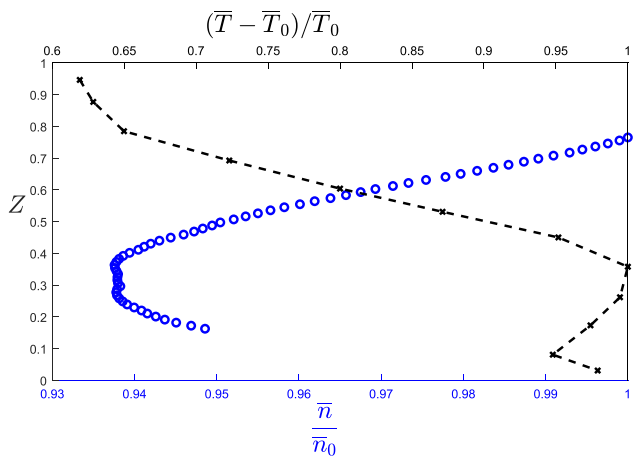


**FIG. 9.** Vertical profiles of the relative normalized mean temperature  $(\bar{T} - \bar{T}_0)/\bar{T}_0$  (black, crosses) and the normalized mean particle number density  $\bar{n}(Y, Z)/\bar{n}_0$  (blue, circles) in the forced convective turbulence averaged over the horizontal region  $Y = 4-15$  cm (near the grid). The coordinate  $Z$  is normalized by  $L_z = 26$  cm.

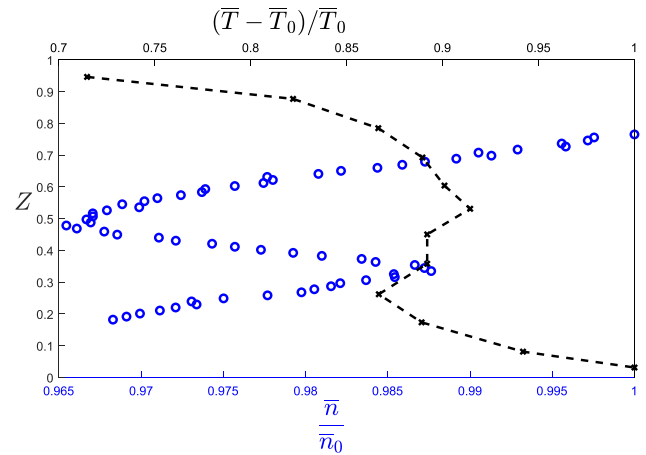


**FIG. 10.** Vertical profiles of the relative normalized mean temperature  $(\bar{T} - \bar{T}_0)/\bar{T}_0$  (black, crosses) and the normalized mean particle number density  $\bar{n}(Y, Z)/\bar{n}_0$  (blue, circles) in the forced convective turbulence averaged over the horizontal region  $Y = 17-24$  cm (far from the grid). The coordinate  $Z$  is normalized by  $L_z = 26$  cm.

been compared with the results of our previous experiments<sup>35,36</sup> conducted in an inhomogeneous and anisotropic stably stratified turbulence<sup>35</sup> produced by a one oscillating grid and in a forced convection with two oscillating grids in the air flow.<sup>36</sup> We have found that contrary to our previous experiments with a forced convection with two oscillating grids,<sup>36</sup> the large-scale circulations in the convective turbulence with a one oscillating grid are not destroyed at a maximum frequency of 10.5 Hz of the grid oscillations, but their structure is deformed (see Fig. 2). The measured vertical turbulent velocities for convective turbulence are stronger than for both, isothermal turbulence and stably stratified turbulence produced by a one oscillating grid, since the buoyancy increases the turbulent kinetic energy for convective turbulence and decreases it for stably stratified turbulence.

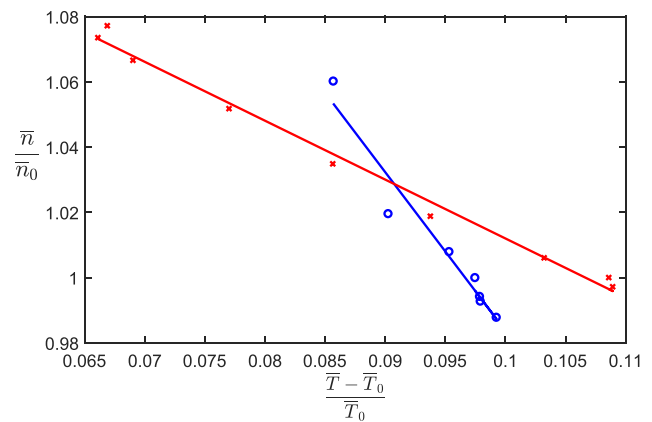


**FIG. 11.** The normalized mean particle number density  $\bar{n}/\bar{n}_0$  vs the relative normalized mean temperature  $(\bar{T} - \bar{T}_0)/\bar{T}_0$  averaged over different horizontal regions:  $Y = 4-15$  cm (blue, circles) with  $\alpha = 4.86$  and  $Y = 16-24$  cm (red, crosses) with  $\alpha = 1.74$  in the forced convective turbulence.

These effects are also observed in the measured vertical integral turbulent length scales obtained from the two-point correlation functions for velocity fluctuations.

To study the phenomenon of turbulent thermal diffusion, we measure spatial distributions of the mean temperature and mean particle number density in many locations. We have found that in the convective turbulence near the grid, the mean temperature increases with the height reaching the maximum and then it decreases nearly linearly with the increase in the height. On the other hand, far from the grid, the behavior of the mean temperature in the convective turbulence is more complicated. The mean fluid temperature decreases with the height reaching the minimum, and for larger heights, it increases with the height reaching the maximum, and finally it decreases nearly linearly with the height (see Fig. 8).

The behavior of the mean particle number density is opposite to the mean temperature. In particular, the mean particle number density increases in the regions where the mean temperature decreases, reaching the maximum nearby the minimum of the mean temperature (see Figs. 9 and 10). This implies that our experiments in convective and stably stratified turbulence with micrometer-size solid particles have clearly demonstrated the existence of the phenomenon of turbulent thermal diffusion, which causes particle accumulation in the vicinity of the minimum of the mean temperature even in a complicated vertical profile of the mean fluid temperature. We have determined the effective turbulent thermal diffusion coefficient using the vertical profiles of the mean temperature and the mean particle number density. We have also demonstrated that the obtained experimental results are in agreement with the theoretical predictions.

## AUTHOR DECLARATIONS

### Conflict of Interest

The authors have no conflicts to disclose.

## Author Contributions

**Elad Elmakies:** conceptualization (equal); data curation (equal); formal analysis (equal); investigation (equal); methodology (equal); validation (equal); visualization (equal); and writing—original draft (equal). **Oleg Shildkrot:** data curation (equal); investigation (equal); and methodology (equal). **Nathan Kleorin:** conceptualization (equal); formal analysis (equal); investigation (equal); methodology (equal); and writing—original draft (equal). **Avi Levy:** conceptualization (equal); formal analysis (equal); investigation (equal); methodology (equal); validation (equal); and writing—original draft (equal). **Igor Rogachevskii:** conceptualization (equal); formal analysis (equal); investigation (equal); methodology (equal); validation (equal); and writing—original draft (equal).

## DATA AVAILABILITY

The data that support the findings of this study are available from the corresponding author upon reasonable request.

## APPENDIX: PARTICLE TURBULENT FLUX FOR SMALL PÉCLET NUMBERS

Here, we derive the expression for the particle turbulent flux for small Péclet numbers. In this case, the nonlinear terms in Eq. (5) for the particle number density fluctuations are much smaller

than the Brownian diffusion term, so we can apply the quasi-linear approach. In the framework of this approach, we neglect the nonlinear terms but keep the molecular diffusion term in Eq. (5). We rewrite Eq. (5) in a Fourier space, i.e., we use the Fourier transform in the  $\mathbf{k}$ - $\omega$  space as follows:

$$n'(t, \mathbf{x}) = \iint n'(\omega, \mathbf{k}) \exp(i\mathbf{k} \cdot \mathbf{x} + i\omega t) d\mathbf{k} d\omega, \quad (\text{A1})$$

$$u_i(t, \mathbf{x}) = \iint u_i(\omega, \mathbf{k}) \exp(i\mathbf{k} \cdot \mathbf{x} + i\omega t) d\mathbf{k} d\omega. \quad (\text{A2})$$

Substituting Eqs. (A1) and (A2) into the linearized equation (5), we obtain

$$\iint \left[ (Dk^2 + i\omega) n'(\omega, \mathbf{k}) + (\nabla_j \bar{n} + i k_j \bar{n}) u_j(\omega, \mathbf{k}) \right] \times \exp(i\mathbf{k} \cdot \mathbf{x} + i\omega t) d\mathbf{k} d\omega = 0. \quad (\text{A3})$$

Therefore, the solution of the linearized equation (5) in the Fourier space is given by

$$n'(\omega, \mathbf{k}) = -G_D(\omega, \mathbf{k}) (\nabla_j \bar{n} + i k_j \bar{n}) u_j(\omega, \mathbf{k}), \quad (\text{A4})$$

where the function  $G_D(\omega, \mathbf{k}) = (Dk^2 + i\omega)^{-1}$ .

Note that Eqs. (A3) and (A4) are not valid in a general case. Nevertheless, we use these equations since

- we take into account in the turbulent particle flux only the effects that are linear in  $\nabla_j \bar{n}$  and neglect higher-order spatial derivatives of the mean particle number density and
- we do not study here the compressibility effects of a turbulent velocity field in the evolution of the mean particle number density (i.e., we do not consider the finite Mach numbers effects).

In this case, we can use Eq. (A4) to determine the turbulent particle flux for small Péclet numbers.<sup>7</sup>

We determine the turbulent particle flux using the multi-scale approach,<sup>39</sup> i.e.,

$$\begin{aligned} \langle n'(t, \mathbf{x}) u_j(t, \mathbf{x}) \rangle &= \lim_{t_1 \rightarrow t_2, \mathbf{x} \rightarrow \mathbf{y}} \langle n'(t_1, \mathbf{x}) u_j(t_2, \mathbf{y}) \rangle \\ &= \lim_{\tau \rightarrow 0, \mathbf{r} \rightarrow 0} \int d\mathbf{k} \int d\omega \langle n'(\omega, \mathbf{k}) u_j(-\omega, -\mathbf{k}) \rangle \\ &\quad \times \exp[i(\mathbf{k} \cdot \mathbf{r} + \omega \tau)] \\ &= \int d\mathbf{k} \int d\omega \langle n'(\omega, \mathbf{k}) u_j(-\omega, -\mathbf{k}) \rangle, \end{aligned} \quad (\text{A5})$$

where  $\mathbf{r} = \mathbf{x} - \mathbf{y}$ ,  $\tau = t_1 - t_2$ , and we consider a homogeneous and stationary (in statistical sense) turbulence. The latter implies that the correlation function  $\langle n'(\omega, \mathbf{k}) u_j(-\omega, -\mathbf{k}) \rangle$  is independent of the large-scale variables. We also assume that there exists a separation of scales, i.e., the maximum scale of random motions  $\ell_0$  is much smaller than the characteristic scales of inhomogeneities of the mean particle number density.

Substituting Eq. (A4) into Eq. (A5), we determine the particle turbulent flux  $\langle u_i n' \rangle$  as

$$\langle u_i n' \rangle = - \int d\mathbf{k} \int d\omega \langle u_i(\omega, \mathbf{k}) u_j(-\omega, -\mathbf{k}) \rangle G_D^* [\nabla_j \bar{n} - i k_j \bar{n}]. \quad (\text{A6})$$



We use the simple model for the second moments,  $\langle u_i(\omega, \mathbf{k}) u_j(-\omega, -\mathbf{k}) \rangle$ , of an isotropic and homogeneous turbulence in the anelastic approximation in a Fourier space as follows:

$$\langle u_i(\omega, \mathbf{k}) u_j(-\omega, -\mathbf{k}) \rangle = \frac{\langle \mathbf{u}^2 \rangle E(k) \Phi(\omega)}{8\pi k^2} \left[ \delta_{ij} - k_{ij} + \frac{i}{k^2} (\lambda_i k_j - \lambda_j k_i) \right], \quad (\text{A7})$$

where the spectrum function  $E(k)$  for the turbulent kinetic energy is  $E(k) = (q-1) k_0^{-1} (k/k_0)^{-q}$  with the exponent  $q$  varying in the interval  $1 < q < 3$ , the interval in the wavenumbers is  $k_0 \leq k \leq k_d$ , and  $k_d \gg k_0$ . The frequency function  $\Phi(\omega)$  is chosen in the form of the Lorentz profile:  $\Phi(\omega) = [\pi \tau_0 (\omega^2 + \tau_0^{-2})]^{-1}$ , where  $\tau_0$  is the correlation time of a random velocity field. This model for the frequency function corresponds to the following non-instantaneous correlation function:  $\langle u_i(t) u_j(t + \tau) \rangle \propto \exp(-\tau/\tau_0)$ . For small Péclet numbers,  $\tau_0 \gg (Dk^2)^{-1}$ . Equation (A7) is derived using symmetry arguments.

Substituting Eq. (A7) into Eq. (A6), we determine the turbulent flux of particles  $\langle u_i n' \rangle$  as

$$\begin{aligned} \langle u_i n' \rangle &= -\frac{\langle \mathbf{u}^2 \rangle}{8\pi} \int_{k_0}^{k_d} E(k) dk \int_0^{2\pi} d\varphi \int_0^\pi \sin \vartheta d\vartheta \\ &\times \left[ \delta_{ij} - k_{ij} + \frac{i}{k^2} (\lambda_i k_j - \lambda_j k_i) \right] [\nabla_j \bar{n} - i k_j \bar{n}] \\ &\times \int G_D^* \Phi(\omega) d\omega = -\frac{\langle \mathbf{u}^2 \rangle}{3D^{(n)}} (\nabla_i \bar{n} + \lambda_i \bar{n}) \int_{k_0}^{k_d} \frac{E(k)}{k^2} dk. \end{aligned} \quad (\text{A8})$$

For the integration over  $\omega$ , we use the following integral:

$$\int_{-\infty}^{\infty} \frac{d\omega}{(\pm i\omega + Dk^2)(\omega^2 + \tau_0^{-2})} = \frac{\pi \tau_0}{\tau_0^{-1} + Dk^2} \approx \frac{\pi \tau_0}{Dk^2}, \quad (\text{A9})$$

which is determined in the limit when the correlation time  $\tau_0 \gg (Dk^2)^{-1}$ . For the integration over  $k$ , we use the following integral:

$$\int_{k_0}^{k_d} \frac{E(k)}{k^2} dk = \frac{q-1}{q+1} \ell_0^2. \quad (\text{A10})$$

After integration over  $\omega$  and in  $\mathbf{k}$ -space in Eqs. (A8), we obtain the formula for the turbulent particle flux  $\langle n' \mathbf{u} \rangle$  as follows:

$$\langle n' \mathbf{u} \rangle = \mathbf{V}^{\text{eff}} \bar{n} - D_T \nabla \bar{n}, \quad (\text{A11})$$

where

$$D_T = \frac{q-1}{3(q+1)} \tau_0 \langle \mathbf{u}^2 \rangle \text{Pe}, \quad (\text{A12})$$

$$\mathbf{V}^{\text{eff}} = -D_T \boldsymbol{\lambda} = D_T \frac{\nabla \bar{\rho}}{\bar{\rho}}. \quad (\text{A13})$$

## REFERENCES

- <sup>1</sup>G. T. Csanady, *Turbulent Diffusion in the Environment* (Reidel, Dordrecht, 1980).
- <sup>2</sup>Y. B. Zeldovich, A. A. Ruzmaikin, and D. D. Sokoloff, *The Almighty Chance* (Word Scientific Publication, Singapore, 1990).
- <sup>3</sup>A. K. Blackadar, *Turbulence and Diffusion in the Atmosphere* (Springer, Berlin, 1997).
- <sup>4</sup>J. H. Seinfeld and S. N. Pandis, *Atmospheric Chemistry and Physics. From Air Pollution to Climate Change*, 2nd ed. (John Wiley & Sons, New York, 2006).
- <sup>5</sup>L. I. Zaichik, V. M. Alipchenkov, and E. G. Sinaiski, *Particles in Turbulent Flows* (John Wiley & Sons, New York, 2008).
- <sup>6</sup>C. T. Crowe, J. D. Schwarzkopf, M. Sommerfeld, and Y. Tsuji, *Multiphase Flows with Droplets and Particles*, 2nd ed. (CRC Press LLC, New York, 2011).
- <sup>7</sup>I. Rogachevskii, *Introduction to Turbulent Transport of Particles, Temperature and Magnetic Fields* (Cambridge University Press, Cambridge, 2021).
- <sup>8</sup>M. Caporaloni, F. Tampieri, F. Trombetti, and O. Vittori, "Transfer of particles in nonisotropic air turbulence," *J. Atmos. Sci.* **32**, 565 (1975).
- <sup>9</sup>M. Reeks, "The transport of discrete particle in inhomogeneous turbulence," *J. Aerosol Sci.* **14**, 729 (1983).
- <sup>10</sup>A. Guha, "A unified Eulerian theory of turbulent deposition to smooth and rough surfaces," *J. Aerosol Sci.* **28**, 1517 (1997).
- <sup>11</sup>T. Elperin, N. Kleorin, and I. Rogachevskii, "Formation of inhomogeneities in two-phase low-Mach-number compressible turbulent fluid flows," *Int. J. Multiphase Flow* **24**, 1163 (1999).
- <sup>12</sup>A. Guha, "Transport and deposition of particles in turbulent and laminar flow," *Annu. Rev. Fluid Mech.* **40**, 311 (2008).
- <sup>13</sup>D. Mitra, N. E. L. Haugen, and I. Rogachevskii, "Turbophoresis in forced inhomogeneous turbulence," *Europ. Phys. J. Plus* **133**, 35 (2018).
- <sup>14</sup>F. De Lillo, M. Cencini, S. Musacchio, and G. Boffetta, "Clustering and turbophoresis in a shear flow without walls," *Phys. Fluids* **28**, 035104 (2016).
- <sup>15</sup>G. Sardina, P. Schlatter, L. Brandt, F. Picano, and C. M. Casciola, "Wall accumulation and spatial localization in particle-laden wall flows," *J. Fluid Mech.* **699**, 50–78 (2012).
- <sup>16</sup>D. Kaftory, G. Hetsroni, and S. Banerjee, "Particle behaviour in the turbulent boundary layer—I: Motion, deposition, and entrainment," *Phys. Fluids* **7**, 1095–1106 (1995).
- <sup>17</sup>M. Righetti and G. P. Romano, "Particle-fluid interactions in a plane near-wall turbulent flow," *J. Fluid Mech.* **505**, 93 (2004).
- <sup>18</sup>T. Elperin, N. Kleorin, and I. Rogachevskii, "Turbulent thermal diffusion of small inertial particles," *Phys. Rev. Lett.* **76**, 224 (1996).
- <sup>19</sup>T. Elperin, N. Kleorin, and I. Rogachevskii, "Turbulent barodiffusion, turbulent thermal diffusion and large-scale instability in gases," *Phys. Rev. E* **55**, 2713 (1997).
- <sup>20</sup>T. Elperin, N. Kleorin, and I. Rogachevskii, "Mechanisms of formation of aerosol and gaseous inhomogeneities in the turbulent atmosphere," *Atmos. Res.* **53**, 117 (2000).
- <sup>21</sup>T. Elperin, N. Kleorin, I. Rogachevskii, and D. Sokoloff, "Passive scalar transport in a random flow with a finite renewal time: Mean-field equations," *Phys. Rev. E* **61**, 2617 (2000).
- <sup>22</sup>T. Elperin, N. Kleorin, I. Rogachevskii, and D. Sokoloff, "Mean-field theory for a passive scalar advected by a turbulent velocity field with a random renewal time," *Phys. Rev. E* **64**, 026304 (2001).
- <sup>23</sup>R. V. R. Pandya and F. Mashayek, "Turbulent thermal diffusion and barodiffusion of passive scalar and dispersed phase of particles in turbulent flows," *Phys. Rev. Lett.* **88**, 044501 (2002).
- <sup>24</sup>M. W. Reeks, "On model equations for particle dispersion in inhomogeneous turbulence," *Int. J. Multiphase Flow* **31**, 93 (2005).
- <sup>25</sup>G. Amir, N. Bar, A. Eidelman, T. Elperin, N. Kleorin, and I. Rogachevskii, "Turbulent thermal diffusion in strongly stratified turbulence: Theory and experiments," *Phys. Rev. Fluids* **2**, 064605 (2017).
- <sup>26</sup>N. E. L. Haugen, N. Kleorin, I. Rogachevskii, and A. Brandenburg, "Detection of turbulent thermal diffusion of particles in numerical simulations," *Phys. Fluids* **24**, 075106 (2012).
- <sup>27</sup>I. Rogachevskii, N. Kleorin, and A. Brandenburg, "Compressibility in turbulent magnetohydrodynamics and passive scalar transport: Mean-field theory," *J. Plasma Phys.* **84**, 735840502 (2018).
- <sup>28</sup>M. Sofiev, V. Sofieva, T. Elperin, N. Kleorin, I. Rogachevskii, and S. S. Zilitinkevich, "Turbulent diffusion and turbulent thermal diffusion of aerosols in stratified atmospheric flows," *J. Geophys. Res.* **114**, D18209, <https://doi.org/10.1029/2009JD011765> (2009).
- <sup>29</sup>T. Elperin, N. Kleorin, M. Podolak, and I. Rogachevskii, "A mechanism for the formation of aerosol concentrations in the atmosphere of Titan," *Planet. Space Sci.* **45**, 923–929 (1997).

- <sup>30</sup>A. Hubbard, "Turbulent thermal diffusion: A way to concentrate dust in protoplanetary discs," *Mon. Notes R. Astron. Soc.* **456**, 3079–3089 (2016).
- <sup>31</sup>J. Buchholz, A. Eidelman, T. Elperin, G. Grünefeld, N. Kleorin, A. Krein, and I. Rogachevskii, "Experimental study of turbulent thermal diffusion in oscillating grids turbulence," *Exp. Fluids* **36**, 879 (2004).
- <sup>32</sup>A. Eidelman, T. Elperin, N. Kleorin, A. Krein, I. Rogachevskii, J. Buchholz, and G. Grünefeld, "Turbulent thermal diffusion of aerosols in geophysics and in laboratory experiments," *Nonlinear Proc. Geophys.* **11**, 343 (2004).
- <sup>33</sup>A. Eidelman, T. Elperin, N. Kleorin, A. Markovich, and I. Rogachevskii, "Experimental detection of turbulent thermal diffusion of aerosols in non-isothermal flows," *Nonlinear Proc. Geophys.* **13**, 109 (2006).
- <sup>34</sup>A. Eidelman, T. Elperin, N. Kleorin, I. Rogachevskii, and I. Sapir-Katiraie, "Turbulent thermal diffusion in a multi-fan turbulence generator with the imposed mean temperature gradient," *Exp. Fluids* **40**, 744 (2006).
- <sup>35</sup>E. Elmakies, O. Shildkrot, N. Kleorin, A. Levy, I. Rogachevskii, and A. Eidelman, "Experimental study of turbulent thermal diffusion of particles in inhomogeneous and anisotropic turbulence," *Phys. Fluids* **34**, 055125 (2022).
- <sup>36</sup>M. Bukai, A. Eidelman, T. Elperin, N. Kleorin, I. Rogachevskii, and I. Sapir-Katiraie, "Transition phenomena in unstably stratified turbulent flows," *Phys. Rev. E* **83**, 036302 (2011).
- <sup>37</sup>S. A. Orszag, "Analytical theories of turbulence," *J. Fluid Mech.* **41**, 363 (1970).
- <sup>38</sup>A. Pouquet, U. Frisch, and J. Leorat, "Strong MHD helical turbulence and the nonlinear dynamo effect," *J. Fluid Mech.* **77**, 321 (1976).
- <sup>39</sup>P. H. Roberts and A. M. Soward, "A unified approach to mean field electrodynamics," *Astron. Nachr.* **296**, 49 (1975).
- <sup>40</sup>A. Brandenburg and K. Subramanian, "Minimal tau approximation and simulations of the alpha effect," *Astron. Astrophys.* **439**, 835 (2005).
- <sup>41</sup>A. Brandenburg, K.-H. Rädler, M. Rheinhardt, and P. J. Käpylä, "Magnetic diffusivity tensor and dynamo effects in rotating and shearing turbulence," *Astrophys. J.* **676**, 740 (2008).
- <sup>42</sup>I. Rogachevskii, N. Kleorin, P. J. Käpylä, and A. Brandenburg, "Pumping velocity in homogeneous helical turbulence with shear," *Phys. Rev. E* **84**, 056314 (2011).
- <sup>43</sup>A. Brandenburg, K.-H. Rädler, and K. Kemel, "Mean-field transport in stratified and/or rotating turbulence," *Astron. Astrophys.* **539**, A35 (2012).
- <sup>44</sup>T. Elperin, N. Kleorin, M. Liberman, A. N. Lipatnikov, I. Rogachevskii, and R. Yu, "Turbulent diffusion of chemically reacting flows: Theory and numerical simulations," *Phys. Rev. E* **96**, 053111 (2017).
- <sup>45</sup>G. I. Taylor, "Diffusion by continuous movements," *Proc. London Math. Soc.* **s2-20**(1), 196–212 (1922).
- <sup>46</sup>P. G. Saffman, "On the effect of the molecular diffusivity in turbulent diffusion," *J. Fluid Mech.* **8**, 273–283 (1960).
- <sup>47</sup>D. Enskog, "Bemerkungen zu einer Fundamentalgleichung in der kinetischen Gastheorie," *Phys. Zs. Leipzig* **12**, 533–539 (1911).
- <sup>48</sup>D. Enskog, "Zur Elektronentheorie der dispersion und absorption der Metalle," *Ann. Phys.* **343**, 731–763 (1912).
- <sup>49</sup>S. Chapman, "The kinetic theory of a gas constituted of spherically symmetrical molecules," *Philos. Trans. R. Soc. London A* **211**, 433–483 (1912).
- <sup>50</sup>M. R. Maxey, "The gravitational settling of aerosol particles in homogeneous turbulence and random flow field," *J. Fluid Mech.* **174**, 441 (1987).
- <sup>51</sup>R. J. Adrian, "Particle-imaging techniques for experimental fluid mechanics," *Annu. Rev. Fluid Mech.* **23**, 261 (1991).
- <sup>52</sup>M. Raffel, C. Willert, S. Werely, and J. Kompenhans, *Particle Image Velocimetry* (Springer, Berlin-Heidelberg, 2007).
- <sup>53</sup>J. Westerweel, "Theoretical analysis of the measurement precision in particle image velocimetry," *Exp. Fluids* **29**, S3 (2000).
- <sup>54</sup>P. Guibert, M. Durget, and M. Murat, "Concentration fields in a confined two-gas mixture and engine in cylinder flow: Laser tomography measurements by Mie scattering," *Exp. Fluids* **31**, 630–642 (2001).
- <sup>55</sup>C. F. Bohren and D. R. Huffman, *Absorption and Scattering of Light by Small Particles* (John Wiley and Sons, New York, 1983).
- <sup>56</sup>M. Bukai, A. Eidelman, T. Elperin, N. Kleorin, I. Rogachevskii, and I. Sapir-Katiraie, "Effect of large-scale coherent structures on turbulent convection," *Phys. Rev. E* **79**, 066302 (2009).
- <sup>57</sup>I. Shimberg, O. Shriki, O. Shildkrot, N. Kleorin, A. Levy, and I. Rogachevskii, "Experimental study of turbulent transport of nanoparticles in convective turbulence," *Phys. Fluids* **34**, 055126 (2022).
- <sup>58</sup>A. Eidelman, T. Elperin, I. Gluzman, N. Kleorin, and I. Rogachevskii, "Experimental study of temperature fluctuations in forced stably stratified turbulent flows," *Phys. Fluids* **25**, 015111 (2013).
- <sup>59</sup>A. Eidelman, T. Elperin, N. Kleorin, B. Melnik, and I. Rogachevskii, "Tangling clustering of inertial particles in stably stratified turbulence," *Phys. Rev. E* **81**, 056313 (2010).
- <sup>60</sup>J. S. Turner, "The influence of molecular diffusivity on turbulent entrainment across a density interface," *J. Fluid Mech.* **33**, 639–656 (1968).
- <sup>61</sup>S. T. Turner, *Buoyancy Effects in Fluids* (Cambridge University Press, Cambridge, 1973).
- <sup>62</sup>S. M. Thompson and J. S. Turner, "Mixing across an interface due to turbulence generated by an oscillating grid," *J. Fluid Mech.* **67**, 349–368 (1975).
- <sup>63</sup>E. J. Hopfinger and J.-A. Toly, "Spatially decaying turbulence and its relation to mixing across density interfaces," *J. Fluid Mech.* **78**, 155–175 (1976).
- <sup>64</sup>E. Kit, E. J. Strang, and H. J. S. Fernando, "Measurement of turbulence near shear-free density interfaces," *J. Fluid Mech.* **334**, 293–314 (1997).
- <sup>65</sup>M. A. Sánchez and J. M. Redondo, "Observations from grid stirred turbulence," *Appl. Sci. Res.* **59**, 243–254 (1997).
- <sup>66</sup>P. Medina, M. A. Sánchez, and J. M. Redondo, "Grid stirred turbulence: Applications to the initiation of sediment motion and lift-off studies," *Phys. Chem. Earth B* **26**, 299–304 (2001).